Magnetoelectric effect and magnetic phase diagram of the polar easy-axis ferrimagnet $CaBaFe_4O_7$

V. Kocsis,[1,2] Y. Tokunaga,[1,3] S. Bordács,[2,4] M. Kriener,[1] A. Puri,[5] U. Zeitler,[5] Y. Taguchi,[1] I. Kézsmárki,[2] and Y. Tokura[1,4,6]

[1]*RIKEN Center for Emergent Matter Science (CEMS), Wako, Saitama 351-0198, Japan*

[2]*Department of Physics, Budapest University of Technology and Economics and MTA-BME Lendület Magneto-optical Spectroscopy Research Group, 1111 Budapest, Hungary*

[3]*Department of Advanced Materials Science, University of Tokyo, Kashiwa 277-8561, Japan*

[4]*Quantum-Phase Electronics Center, Department of Applied Physics, University of Tokyo, Tokyo 113-8656, Japan*

[5]*High Field Magnet Laboratory (HFML-EMFL), Radboud University Nijmegen, Toernooiveld 7, 6525 ED Nijmegen, The Netherlands*

[6]*Department of Applied Physics, University of Tokyo, Hongo, Tokyo 113-8656, Japan*

Abstract

The magnetic phase diagram of the polar easy-axis ferrimagnet $CaBaFe_4O_7$ has been investigated by magnetization, specific heat, and magnetoelectric measurements. The ferrimagnetic transition takes place at T_{C1}=275 K within the orthorhombic phase followed by a second magnetic transition at T_{C2}=211 K. Below T_{C2}, successive metamagnetic transitions occur for magnetic fields applied perpendicular to the easy axis, implying a sequence of magnetic states which are neither collinear nor coplanar. The observation of the static magnetoelectric effect was limited to temperatures below 120 K due to the conducting nature of the crystals at higher temperatures. The magnitude of the ferroelectric polarization shows large changes between the different field-induced magnetic phases. The low-field state is characterized by a large linear magnetoelectric coefficient of α_{cc} =39 ps/m, while a gigantic polarization change of ΔP=850 μC/m^2 was observed for $\mu_o H$=14 T applied along the easy axis.

PACS numbers: 75.85.+t, 75.30.Kz, 81.30.Bx

I. INTRODUCTION

The magnetoelectric (ME) effect, which is a consequence of the cross-coupling between spin and charge degrees of freedom, is one of the most desired properties of materials for modern applications. In a magnetoelectric material, the magnetization can be changed by the application of an electric field and the electric polarization can be controlled by a magnetic field.[1–7] Such materials are promising for the development of low-power consumption spintronics, non-volatile ME data storage,[8,9] optical diodes,[10,11] and high-sensitivity ac magnetic field sensors.[12] Recently strong efforts have been focused on the fundamental understanding of multiferroicity in well-known material classes, such as the perovskite-related oxides[2–4,6,7], akermanites[10,13–15], hexaferrites[16], and the polar skyrmion-host lacunar spinels.[17,18] However, $BiFeO_3$ is still the only well-characterized room-temperature multiferroic compound,[19–21] which triggers a chase for new materials possibly exhibiting multiferroicity near room temperature. *Swedenborgites* represent a new class of polar magnets where the long range ferrimagnetic order occurs at relatively high temperatures.[22,23]

The investigation of magnetoelectric effects in $CaBaFe_4O_7$, the target material of the present study, is partly motivated by the strong magnetoelectric coupling reported in $CaBaCo_4O_7$.[24,25] A giant polarization change of ΔP=17000 μC/m^2 was observed along the c axis in $CaBaCo_4O_7$ across the transition from the pyroelectric paramagnetic state to the pyroelectric ferrimagnetic phase at T_C=64 K.[25] *Ab initio* calculations combined with Landau theory showed that the electric polarization change can be attributed to exchange-striction effects.[26] A similar polarization change of magnetoelastic origin is expected in the case of $CaBaFe_4O_7$. Moreover, in $CaBaFe_4O_7$ the magnetic ordering takes place near room temperature,[23] T_{C1}=275 K, which is a good starting point to further enhance the temperature of the magnetic phase transition by fine-tuning the material composition.

Other interesting aspects of this material are its polar structure and the coexistence of different geometrically frustrated sublattices occupied with mixed valence iron ions. As explained in details below, the structure of ABM_4O_7 *Swedenborgites* is polar along the c axis, and consists of a stacking of alternating triangular- and kagome-layers of the magnetic M ions. The nominal valence state of the transition metal (M) is 2.5+, which may imply

that M^{2+} and M^{3+} ions in a 1 : 1 ratio are distributed among the triangular and kagome-layers, respectively. Shorter oxygen-oxygen bonds were reported[23,27,28] around the metal ions in the triangular layers, indicating that one of the two extra holes is localized on the triangular-lattice plane, and the other hole is distributed over the three inequivalent sites in the kagome-layer. Furthermore, the presence of charge order was suggested based on the rapid increase of electrical resistivity towards lower temperatures.[29–31] Although the onset of charge order is still an open issue in $CaBaFe_4O_7$ and $CaBaCo_4O_7$, it may have a strong influence on the dielectric properties of the system.

Due to the mixed valency of the magnetic ions in *Swedenborgites*, charge ordering, if occurs, can strongly influence the spin order. $CaBaFe_4O_7$ and $CaBaCo_4O_7$ are the only memebers of this material family where long-range three-dimensional magnetic order has been reported.[22,23,28] In $CaBaCo_4O_7$, first-principles calculations suggested that the strong orthorhombic distortion of the structure may partially release the geometrical frustration, leading to a ferrimagnetic order.[32,33] The orthorhombic distortion in $CaBaCo_4O_7$ may be induced by the Jahn-Teller active Co^{3+} ions with $e^3\,t_2^3$ configurations. This scenario is supported by the different temperature evolution of Co – O bond-lengths at different Co sites.[32] In its sister compounds with hexagonal symmetry—such as $YbBaCo_4O_7$, $Ca_{0.5}Y_{0.5}BaCo_4O_7$, and $YBaFe_4O_7$—the strong geometrical frustration fully suppresses the long-range magnetic order, and they exhibit spin-glass or spin-liquid ground state.[28,34–39] The complex and subtle nature of the magnetic state in these materials is well exemplified by the case of $YBaCo_4O_7$, which shows no long-range magnetic order, though its orthorhombic distortion should reduce the geometrical frustration of magnetic interactions.[40–42]

The orthorhombic structural unit cell of $CaBaFe_4O_7$ with space group $Pbn2_1$,[23] shown in Fig. 1(a), is composed of four formula units. Although $CaBaFe_4O_7$ is orthorhombic at room temperature, we describe the main characteristics of its structure in comparison with its hypothetic high symmetry form, the polar hexagonal $P6_3mc$ structure, which is often realized in its sister compounds with solid solution of different transition metal ions at the M sites.[38,39,43,44] The structure of ABM_4O_7 generally consists of a stacking of alternating kagome–triangular–kagome–triangular (KTKT) layers of magnetic M ions with tetrahedral oxygen coordination. The corner-sharing oxygen tetrahedra are oriented with one vertex along the stacking direction of the KTKT layers, while the remaining three vertices lie in the ab plane and are linked to those of neighboring tetrahedra, thereby giving rise to the

polar structure. Adjacent kagome layers within KTKT units are rotated by 180 degree around the c axis with respect to each other, forming voids which are filled with the A and B cations. The stability of this structure is related not only to the size of the void and the ionic radii of the A and B cations, but also to the valence state of the M ions.[39,42,45] For example, in case of $CaBaCo_4O_7$, the presence of the Jahn-Teller active Co^{3+} ions leads to a structural phase transition to the $Pbn2_1$ orthorhombic symmetry by buckling and distortion of the CoO_4 tetrahedra. In $CaBaFe_4O_7$ Jahn-Teller distortion can emerge for the Fe^{2+} ions. The same structure was reported earlier for $CaBaFe_4O_7$,[23] where buckling of the FeO_4 tetrahedra leads to a rotation of the Fe1-O_4 (green) tetrahedra and the asymmetry of the triangles formed by Fe2-O_4, Fe3-O_4, Fe4-O_4 tetrahedra, as shown in Fig. 1(b).

The primary purpose of this work is to investigate the complex magnetic structure of $CaBaFe_4O_7$ by revealing the magnetic phase diagram with the use of melt-grown crystals. As a further step, we present evidence for the large static magnetoelectric effect, which may arise from the interplay between the non-collinear and non-coplanar spin patterns, the magnetostriction and the mixed valency of the iron ions.

II. EXPERIMENTAL TECHNIQUES

A. Sample preparation and characterization

High quality $CaBaFe_4O_7$ crystals were prepared by a conventional floating zone technique. As a first step, polycrystalline form of $CaBaFe_4O_7$ was prepared by a series of solid-state reactions. The main difficulty in the preparation of $CaBaFe_4O_7$ arises from the mixed valence nature (Fe^{2+} and Fe^{3+}) of the target compound. In the sintering process, the average 2.5+ valence state of the Fe ions was ensured by using proper 2 : 1 stochiometric ratio of FeO and Fe_2O_3 of the starting materials. Stochiometric amounts of $CaCO_3$, $BaCO_3$, FeO, and Fe_2O_3 were mixed and calcined in high-purity argon atmosphere for 12 h at 1000°C, and after homogenization, the powder was further treated at 1100°C in high-vacuum atmosphere for 24 h. The resultant material was pressed into a rod, which was further sintered at 1000°C in a reducing Ar+3%H_2 atmosphere for 12 h. Single crystals were grown in flowing N_2 atmosphere by an optical imaging floating-zone apparatus.

The material was verified to be of single phase by powder X-ray diffraction and the

crystal orientation was determined by Laue-diffraction patterns. While the c axis is unique in our crystals, polarized optical microscopy showed the presence of structural twins with different orientations of the a and b axis. Magnetization and dielectric polarization measurements confirmed this observation, as no apparent anisotropy was detected in the ab plane. Therefore, in the macroscopic quantities the structural twinning effectively masks the orthorhombicity and restores the hexagonal symmetry of the crystals.

B. Measurement techniques

Magnetization measurements up to $\mu_o H$=14 T and 32 T were respectively carried out in a Physical Property Measurement System (Quantum Design) and at the High Field Magnetic Laboratory (HFML) in Nijmegen, using the vibrating sample magnetometer method in both cases. Specific heat was measured by a Physical Property Measurement System (Quantum Design), applying a relaxation method in the temperature range of T=2-300 K, while for T=150-600 K a Netzsch DSC 200 F3 differential scanning calorimeter equipped with a TASC 414/4 temperature controller was used.

Electric polarization measurements were performed on samples with typical dimensions of $0.5 \times 4 \times 4\,\mathrm{mm}^3$ with a Keithley 6517A electrometer. Effective electric poling was practically prohibited, due to the high conductivity of the crystals even at T_{C2}. As a consequence, it was not possible to investigate the influence of magnetic ordering on the electric properties by means of pyro-current measurements. Instead, we carried out magneto-current measurements at fixed temperatures below T=120 K. (Above this temperature, leakage currents prevented the accurate measurement of field-induced polarization). The magnetically induced polarization was determined by the integration of the magneto-current curves.

III. RESULTS AND DISCUSSIONS

A. Magnetic properties

Fig. 2 shows the field dependence of the magnetization at low temperatures. In contrast to the easy-plane ferrimagnetic character of $CaBaCo_4O_7$[22,32], $CaBaFe_4O_7$ is an easy-axis ferrimagnet with a spontaneous magnetization pointing along the c axis.[23] The

remanent magnetization is M_c^{Rem} ≈2.5 μ_B/f.u., which is remarkably large compared to other compounds in the *Swedenborgite* family. For magnetic fields applied along the easy axis, following a narrow hysteresis the magnetization reaches the value of ∼5.1 μ_B/f.u. In the field range of $\mu_o H$=14-28 T, there is a broad magnetization plateau characterized by a slightly larger moment of M_c^{Sat} ≈5.5 μ_B/f.u. This value corresponds to about 1/3 of the magnetization in the fully polarized state (18 μ_B/f.u.).

For magnetic fields applied perpendicular to the c axis, successive metamagnetic transitions are observed between $\mu_o H$=1 and 14.5 T at T=2 K (see also Fig. 5(d) and Fig. 6(e)). Due to their broad hysteresis the subsequent metamagnetic transitions overlap with each other and it is not possible to unambiguously determine their critical field values, though their overlaps are reduced towards higher temperatures as can be followed in Fig. 6(e). Hereafter, we will refer to this field range as the metamagnetic region bound by a lower critical field $\mu_o H_{\mathrm{C3}}$ and an upper critical field $\mu_o H_{\mathrm{C4}}$. Above this field range the magnetization nearly approaches the value found for fields parallel to the easy axis, which indicates that the Zeeman energy overcomes the effect of easy-axis anisotropy for $\mu_o H \gtrsim$15 T.

Figure 3 shows the temperature dependence of the magnetization measured in $\mu_o H$=1 T and the zero-field specific heat. Three transitions are manifested in the specific heat measurements at T_{S}=380 K, T_{C1}=275 K, and T_{C2}=211 K. The anomaly at T_{S}=380 K likely indicates a structural transition as the material is still paramagnetic at this temperature. The other two transitions at T_{C1}=275 K and T_{C2}=211 K, formerly described as a ferrimagnetic and a spin re-orientation transition,[23,46,47] show up in the magnetization curves. At T_{C2} there is only a weak anomaly in the magnetization measured in $\mu_o H$=1 T applied within the *ab* plane.

Fig. 4 shows the inverse magnetic susceptibilities around and above room temperature, which were measured in $\mu_o H$=0.3 T magnetic field applied along and perpendicular to the c axis. The magnetic anisotropy persists up to temperatures well above T_{S}=380 K reflecting the hexagonal symmetry of the crystal. For both orientations of the magnetic field the susceptibility curves exhibit anomalies near T_{S}=380 K, the temperature of the structural transition as determined from the zero-field specific heat measurement, and a broad hysteresis below this temperature. By fitting the c axis and *ab* plane susceptibilities

with the Curie-Weiss law in the limited temperature range of T=500-600 K one obtains θ_c=-2150 K and θ_{ab}=-2050 K, respectively, which point to an overall strong antiferromagnetic coupling among the Fe^{2+} and Fe^{3+} magnetic moments. The relatively large value of θ/T_{C1} ≈7.7 indicates the frustrated nature of the magnetic interactions.

The effective magnetic moments obtained for field parallel and perpendicular to the c axis, $\mu_{\mathrm{eff},c}$=22 μ_B/f.u. and $\mu_{\mathrm{eff},ab}$=20.4 μ_B/f.u. are nearly comparable with the value $2\times(2\cdot\sqrt{2\cdot 3}+2\cdot\sqrt{\frac{5}{2}\cdot\frac{7}{2}})\,\mu_B$/f.u.=21.6 μ_B/f.u. expected for the four mixed-valence Fe ions per formula unit. The frustrated antiferromagnetic interactions, together with the saturation moment of M_c^{Sat} ≈5.5 μ_B/f.u., is indicative of a non-collinear or non-coplanar magnetic structure, as already proposed in a former X-ray magnetic circular dichroism study.[23]

B. Magnetoelectric properties

Figure 5 summarizes the magnetic field dependence of different components of the ferroelectric polarization at T=80 K for different orientations of the magnetic field. For a direct comparison between the magnetic and magnetoelectric properties of $CaBaFe_4O_7$, the corresponding magnetization data are simultaneously plotted in the lower panels of the figure.

Figure 5(a) shows the field-induced polarization ΔP when the magnetic field is applied along the c axis. The polarization component parallel to the field is as large as ΔP=850 μC/m^2 in $\mu_o H$=14 T, while the polarization component perpendicular to the field is negligible. In low fields, the former is proportional to the field and the corresponding linear magnetoelectric coefficient is α_{cc} ≈39 ps/m. The hysteresis of the magnetization around zero field is accompanied with a butterfly-shape hysteresis[48] of the polarization (see the inset of Fig 5(a)). In the magnetization curve a weak hysteresis is found to persist up to higher fields, as shown in the inset of Fig 5(c), which is more clearly manifested in the polarization.

Figure 5(b) displays ΔP when the magnetic field is applied within the ab plane. In this configuration, finite polarizations can be observed in all the three independent configurations, though the dominant component is again the one parallel to the easy axis. In this component, the largest changes, as high as ΔP ≈ - 400 μC/m^2, are observed in the field range of the metamagnetic region. The successive magnetic transitions are accompanied with sudden changes in all the three components of the polarization (see the inset of Fig 5(b)).

Figure 6 shows the three largest terms in the magnetically induced polarization at various temperatures below T=120 K together with the corresponding magnetization curves measured for fields along and perpendicular to the easy axis. Figure 6(a) shows the polarization component along the c axis when the magnetic field is applied along the same direction. At each temperature, the polarization shows a butterfly-shape hysteresis at low fields as previously shown in Fig 5(a) for T=80 K. The linear magnetoelectric susceptibility at $\mu_o H$=0 T shows a sign change at around T=30 K. The hysteresis is the largest at T=80 K, and almost vanishes at T=120 K similarly to the hysteresis observed in the corresponding magnetization curves (see the inset of Fig. 6(d)).

Figure 6(b) displays the polarization component along the c axis at various temperatures for transverse magnetic field. While the low-field state exhibits negligible polarization change, abrupt variations in the induced polarization occur at the metamagnetic transitions. The hysteresis loops observed in the polarization coincide with those found in the magnetization. Finally, Fig. 6(c) shows the polarization component measured parallel to the magnetic field when both were perpendicular to the c axis. This polarization term is smaller than the other two and exhibits a rather complex field dependence over the range of the metamagnetic transitions.

For comparison with other ME materials, in Fig. 7(a) we show the temperature evolution of the linear magnetoelectric coefficients $\alpha_{cc} = \partial P_c/\partial H_c$ and $\alpha_{aa} = \partial P_a/\partial H_a$. While the α_{cc} magnetoelectric tensor component reaches its maximum value of $\alpha_{cc} \approx$39 ps/m at T=80 K, the other component peaks at low-temperatures with $\alpha_{aa} \approx$31 ps/m at T=20 K. These values are as large as that of $TbPO_4$ with $\alpha_{aa} \approx$37 ps/m[49] and that of $LiCoPO_4$ with α_{ba}=30.6 ps/m.[50]

Figure 7(b) displays the temperature dependence of the magnetically induced polarization in constant magnetic fields. Representative field values were chosen to trace thermal features associated with the largest magnetically induced polarization terms. The polarization components has a maximum at around T=80 K irrespective of the orientation of the magnetic field. The polarization component, which is perpendicular to the c axis and parallel to the magnetic field, monotonously decreases with increasing temperature and changes sign at about 80 K.

C. $\mu_o H - T$ phase diagram

Based on the temperature- and field-dependent magnetization, magnetoelectric and specific heat measurements we have constructed the magnetic phase diagram of $CaBaFe_4O_7$[51]. Figure 8(a) and (b) present the $\mu_o H - T$ phase diagram for magnetic fields parallel and perpendicular to the c axis. Below T_{C1}=275 K, we find a ferrimagnetic phase characterized by an easy-axis anisotropy. In finite magnetic fields applied parallel to the c axis, the paramagnetic to ferrimagnetic transition becomes a crossover, which shifts to higher temperatures with increasing magnetic field. Color gradation is used to indicate the finite-field crossover line connected to the magnetic phase transition observed at T_{C1}=275 K in zero field. In contrast, for magnetic fields perpendicular to the c axis the transition remains sharp and is rapidly suppressed in finite fields forming the phase boundary $\mu_o H_{C1}(T)$.

The second zero-field transition at around T_{C2}=211 K is resolved in the magnetization as well as in the specific heat measurements. In finite magnetic fields this transition point evolves to an extended phase boundary, where the corresponding transition lines are labeled as $\mu_o H^{\parallel}_{C2}(T)$ and $\mu_o H^{\perp}_{C2}(T)$ for fields parallel and perpendicular to the c axis, respectively. Here we note that $\mu_o H^{\perp}_{C2}(T)$ shows up only in specific heat data and remains indiscernible in the magnetization measurements in low fields, namely up to its crossing with $\mu_o H_{C1}(T)$. As discussed earlier and documented in Fig. 6 in details, for $T < T_{C2}$ there is a sequence of metamagnetic transitions located below $\mu_o H^{\perp}_{C2}(T)$, when the magnetic field is applied perpendicular to the c axis. This metamagnetic region is bound by $\mu_o H_{C3}(T)$ and $\mu_o H_{C4}(T)$. The transition line $\mu_o H_{C3}(T)$ is characterized by a large hysteresis.

IV. CONCLUSIONS

Melt-grown crystals of the orthorhombic polar ferrimagnet $CaBaFe_4O_7$ have been synthesized with the optical floating zone technique. Based on the combined magnetization, calorimetric, and magnetoelectric measurements, we have mapped out the $\mu_o H - T$ magnetic phase diagram of the material. Specific heat measurements revealed a structural phase transition to a higher symmetry form of $CaBaFe_4O_7$ takes place at T_S=380 K. We found a paramagnetic to ferrimagnetic transition at T_{C1}=275 K followed by a spin re-ordering transition at T_{C2}=211 K. Below T_{C2} magnetic fields applied perpendicular to the c axis drive

the system through a cascade of metamagnetic transitions. While the spin patterns in the different phases cannot be determined from the present data, we explored the magnetic phase diagram in fine details for magnetic fields applied both along and perpendicular to the easy axis. In addition, we have investigated the magnetoelectric properties below T_{C2} with different orientations of the magnetic field. A large linear magnetoelectric coefficient of $\alpha_{cc} \approx 39\,\mathrm{ps/m}$ as well as a gigantic field-induced polarization of $\Delta P = 850\,\mu\mathrm{C/m^2}$ have been observed for magnetic fields along the c axis. The magnetic phase diagram together with the observed magnetoelectric effect establish a good starting point to develop a microscopic description of the coupling between spin and charge degrees of freedom in $CaBaFe_4O_7$, a novel nearly room-temperature multiferroic oxide. However, the low symmetry of the crystal structure does not allow the identification of the microscopic origin of the magnetoelectric coupling at the present stage. Determination of the magnetic structure in the different magnetic phases together with *ab initio* calculations could complement our study to assign whether the magnetically induced polarization is governed by magnetostriction, by the spin-current mechanism or by spin-dependent orbital hybridization between the irons and their oxygen ligands.

Acknowledgments

The authors are grateful for the technical assistance provided by A. Kikkawa and T. Suzuki, and for the fruitful discussion with I. Lovas. This work was supported by the Funding Program for World-Leading Innovative R&D on Science and Technology (FIRST Program) on 'Quantum Science on Strong Correlation' from JSPS and by the Hungarian Research Funds OTKA K 108918, OTKA PD 111756 and Bolyai 00565/14/11. We acknowledge the support of the HFML-RU/FOM, member of the European Magnetic Field Laboratory (EMFL). M. K. is supported by a Grants-in-Aid for Young Scientists (B) (JSPS, KAKENHI No. 25800197) and by a Grants-in-Aid for Scientific Research (C) (JSPS, KAKENHI No. 15K05140).

---

[1] D. N. Astrov, Sov. Phys. JETP **13**, 729 (1961).

[2] T. Kimura, T. Goto, H. Shintani, K. Ishizaka, T. Arima, and Y. Y. Tokura, Nature **426**, 55 (2003).

[3] N. Hur, P. A. Sharma, J. S. Ahn, S. Guha, and S.-W. Cheong, Nature **429**, 392 (2004).

[4] M. Fiebig, J. Phys. D: Appl. Phys. **38**, R123 (2005).

[5] S.-W. Cheong and M. Mostovoy, Nature Materials **6**, 13 (2007).

[6] Y. Tokunaga, Y. Taguchi, T.-h. Arima, and Y. Tokura, Nature Physics **8**, 838 (2012).

[7] Y. Tokura, S. Seki, and N. Nagaosa, Reports on Progress in Physics **77**, 076501 (2014).

[8] R. Ramesh, R. and N. A. Spaldin, Nature Materials **6**, 21 (2007).

[9] L. W. Martin, Y.-H. Chu, and R. Ramesh, Materials Science and Engineering: R: Reports **68**, 89 (2010).

[10] I. Kézsmárki, D. Szaller, S. Bordács, V. Kocsis, Y. Tokunaga, Y. Taguchi, H. Murakawa, Y. Tokura, H. Engelkamp, T. Rõõm, and U. Nagel, Nature Communications **5**, 3203 (2014).

[11] I. Kézsmárki, U. Nagel, S. Bordács, R. S. Fishman, J. H. Lee, H. T. Yi, S.-W. Cheong, and T. Rõ om, Physical Review Letters **115**, 127203 (2015).

[12] V. E. Wood and A. E. Austin, International Journal of Magnetism **5**, 303 (1973).

[13] H. Murakawa, Y. Onose, S. Miyahara, N. Furukawa, and Y. Tokura, Physical Review Letters **105**, 137202 (2010).

[14] M. Akaki, H. Iwamoto, T. Kihara, M. Tokunaga, and H. Kuwahara, Physical Review B **86**, 060413 (2012).

[15] S. Bordács, I. Kézsmárki, D. Szaller, L. Demkó, N. Kida, H. Murakawa, Y. Onose, R. Shimano, T. Rõõm, U. Nagel, S. Miyahara, N. Furukawa, and Y. Tokura, Nature Physics **8**, 734 (2012).

[16] T. Kimura, Annu. Rev. Condens. Matter Phys. **3**, 93 (2012).

[17] I. Kézsmárki, S. Bordács, P. Milde, E. Neuber, L. M. Eng, J. S. White, H. M. Rønnow, C. D. Dewhurst, M. Mochizuki, K. Yanai, H. Nakamura, D. Ehlers, V. Tsurkan, and A. Loidl, Nature Materials **14**, 1116 (2015).

[18] E. Ruff, S. Widmann, P. Lunkenheimer, V. Tsurkan, S. Bordács, I. Kézsmárki, and L. A., arXiv:1504.00309 [cond-mat.str-el] (2015).

[19] J. Wang, J. B. Neaton, H. Zheng, V. Nagarajan, S. B. Ogale, B. Liu, D. Viehland, V. Vaithyanathan, D. G. Schlom, U. V. Waghmare, N. A. Spaldin, K. M. Rabe, M. Wuttig, and R. Ramesh, Science **299**, 1719 (2003).

[20] S. Lee, W. Ratcliff, S.-W. Cheong, and V. Kiryukhin, Applied Physics Letters **92**, 192906

(2008).

[21] M. Tokunaga, M. Akaki, T. Ito, S. Miyahara, A. Miyake, H. Kuwahara, and N. Furukawa, Nature Communications **6**, 5878 (2015).

[22] V. Caignaert, V. Pralong, A. Maignan, and B. Raveau, Solid State Communications **149**, 453 (2009).

[23] N. Hollmann, M. Valldor, H. Wu, Z. Hu, N. Qureshi, T. Willers, Y.-Y. Chin, J. C. Cezar, A. Tanaka, N. B. Brookes, and L. H. Tjeng, Physical Review B **83**, 180405 (2011).

[24] K. Singh, V. Caignaert, L. C. Chapon, V. Pralong, B. Raveau, and A. Maignan, Physical Review B **86**, 024410 (2012).

[25] V. Caignaert, A. Maignan, K. Singh, C. Simon, V. Pralong, B. Raveau, J. F. Mitchell, H. Zheng, A. Huq, and L. C. Chapon, Physical Review B **88**, 174403 (2013).

[26] R. D. Johnson, K. Cao, F. Giustino, and P. G. Radaelli, Physical Review B **90**, 045129 (2014).

[27] V. Caignaert, A. M. Abakumov, D. Pelloquin, V. Pralong, A. Maignan, G. V. Tendeloo, and B. Raveau, Chemistry of Materials **21**, 1116 (2009).

[28] W. Schweika, M. Valldor, and P. Lemmens, Physical Review Letters **98**, 067201 (2007).

[29] H. Hao, C. Chen, L. Pan, J. Gao, and X. Hu, Physica B: Condensed Matter **387**, 98 (2007).

[30] N. Nakayama, T. Mizota, Y. Ueda, A. Sokolov, and A. Vasiliev, Journal of Magnetism and Magnetic Materials **300**, 98 (2006), the third Moscow International Symposium on Magnetism 2005The third Moscow International Symposium on Magnetism 2005.

[31] H. Hao, Q. He, Y. Cheng, and L. Zhao, Journal of Physics and Chemistry of Solids **75**, 495 (2014).

[32] V. Caignaert, V. Pralong, V. Hardy, C. Ritter, and B. Raveau, Physical Review B **81**, 094417 (2010).

[33] S. Chatterjee and T. Saha-Dasgupta, Physical Review B **84**, 085116 (2011).

[34] A. Huq, J. Mitchell, H. Zheng, L. Chapon, P. Radaelli, K. Knight, and P. Stephens, Journal of Solid State Chemistry **179**, 1136 (2006).

[35] A. Maignan, V. Caignaert, D. Pelloquin, S. Hébert, V. Pralong, J. Hejtmanek, and D. Khomskii, Physical Review B **74**, 165110 (2006).

[36] V. Caignaert, A. Maignan, V. Pralong, S. Hébert, and D. Pelloquin, Solid State Sciences **8**, 1160 (2006).

[37] D. D. Khalyavin, P. Manuel, B. Ouladdiaf, A. Huq, P. W. Stephens, H. Zheng, J. F. Mitchell,

and L. C. Chapon, Physical Review B **83**, 094412 (2011).

[38] M. Valldor, Solid State Sciences **6**, 251 (2004).

[39] M. Valldor, N. Hollmann, J. Hemberger, and J. A. Mydosh, Physical Review B **78**, 024408 (2008).

[40] M. Soda, Y. Yasui, T. Moyoshi, M. Sato, N. Igawa, and K. Kakurai, Journal of the Physical Society of Japan **75**, 054707 (2006).

[41] L. C. Chapon, P. G. Radaelli, H. Zheng, and J. F. Mitchell, Physical Review B **74**, 172401 (2006).

[42] T. Sarkar, V. Pralong, V. Caignaert, and B. Raveau, Chemistry of Materials **22**, 2885 (2010).

[43] M. Valldor, R. P. Hermann, J. Wuttke, M. Zamponi, and W. Schweika, Physical Review B **84**, 224426 (2011).

[44] M. Valldor and O. Breunig, Solid State Sciences **13**, 831 (2011).

[45] T. Sarkar, V. Caignaert, V. Pralong, and B. Raveau, Journal of Superconductivity and Novel Magnetism **25**, 627 (2012).

[46] B. Raveau, V. Caignaert, V. Pralong, D. Pelloquin, and A. Maignan, Chemistry of Materials **20**, 6295 (2008).

[47] K. Vijayanandhini, C. Simon, V. Pralong, V. Caignaert, and B. Raveau, Physical Review B **79**, 224407 (2009).

[48] E. Ascher, H. Rieder, H. Schmid, and H. Stössel, Journal of Applied Physics **37**, 1404 (1966).

[49] G. T. Rado, J. M. Ferrari, and W. G. Maisch, Physical Review B **29**, 4041 (1984).

[50] I. Kornev, M. Bichurin, J.-P. Rivera, S. Gentil, H. Schmid, A. G. M. Jansen, and P. Wyder, Physical Review B **62**, 12247 (2000).

[51] J. Cardy, *Scaling and renormalization in statistical physics*, Vol. 5 (Cambridge University Press, 1996).

[52] K. Momma and F. Izumi, Journal of Applied Crystallography **41**, 653 (2008).

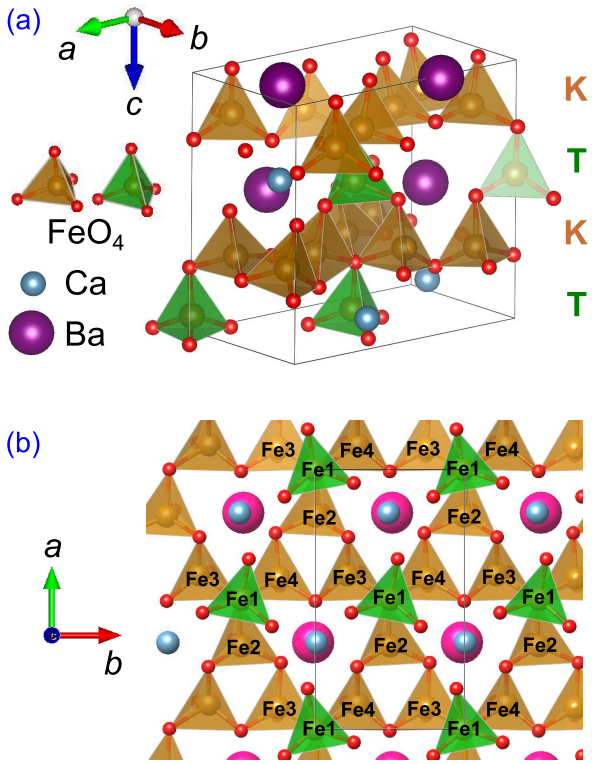

FIG. 1: (Color online) (a) Orthorombic unit cell of $CaBaFe_4O_7$ composed of 4 formula units. FeO_4 tetrahedra belonging to the alternating kagome- and triangular-layers are indicated by brown and green colors, respectively.[23,52] The divalent Ca and Ba cations are located on top of each other in the voids of the stacking layers. (b) One kagome- and triangular-layer as viewed from the crystallographic c direction. The asymmetric shape of the tetrahedra their misorientation relative to the regular triangular and kagome lattice and the relative displacement of the Ca and Ba ions in the ab plane are the consequences of the orthorhombic distortion.

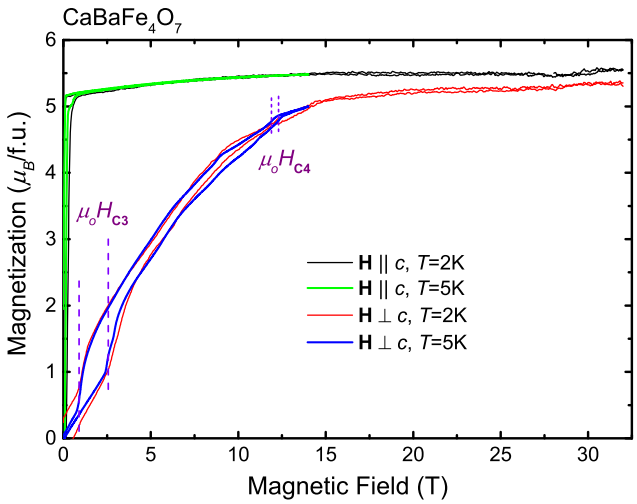

FIG. 2: (Color online) Magnetic-field dependence of the magnetization measured in the low-temperature phase of $CaBaFe_4O_7$ for magnetic fields parallel (black and green) and perpendicular (red and blue) to the c direction up to $\mu_o H$=32 T. The borders of the metamagnetic transitions are labeled by the $\mu_o H^*_{C3}$ lower critical and the $\mu_o H^*_{C4}$ upper critical fields, showing up for H$\perp$ c. Both are characterized by finite hysteresis.

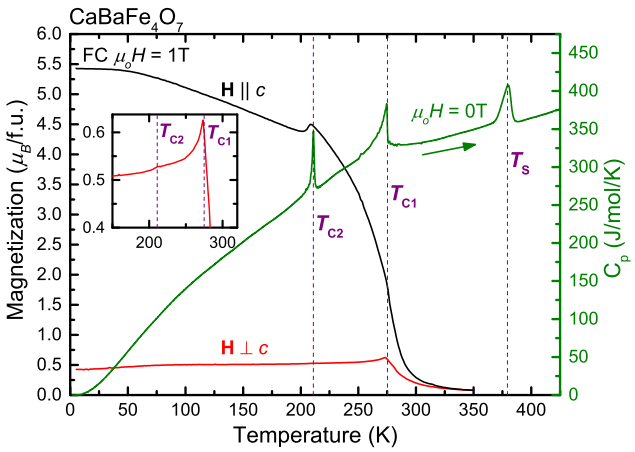

FIG. 3: (Color online) Temperature dependence of the magnetization in field-cooling (FC) with $\mu_o H$=1 T applied along and perpendicular to the c direction, and the specific heat of $CaBaFe_4O_7$ in zero-field in a warming run. Three phase transitions are observed in the specific heat among which to one at T_S=380 K is likely to be of structural origin. The other two transitions are strongly manifested in the magnetization as well. T_{C1}=275 K is the Curie-temperature of the ferrimagnetic ordering, and T_{C2}=211 K is a second magnetic transition, where magnetization along the c axis decreases slightly. The inset shows an magnified view of the magnetization in field-cooling run around T_{C1} and T_{C2} with $\mathbf{H} \perp c$.

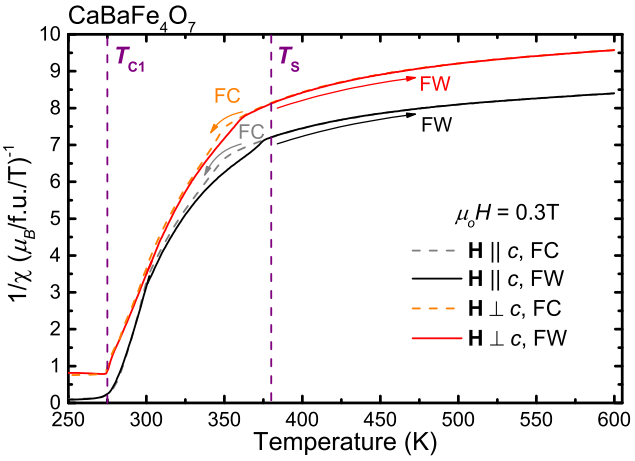

FIG. 4: (Color online) Curie plot of the high temperature magnetic susceptibility of $CaBaFe_4O_7$ with magnetic fields applied along and perpendicular to the c axis, in field-cooling (FC) and field-warming (FW) runs. Vertical dashed lines indicate the structural transition temperature (T_S) as determined from the zero-field the specific heat measurements and the ferrimagnetic transition temperature (T_{C1}).

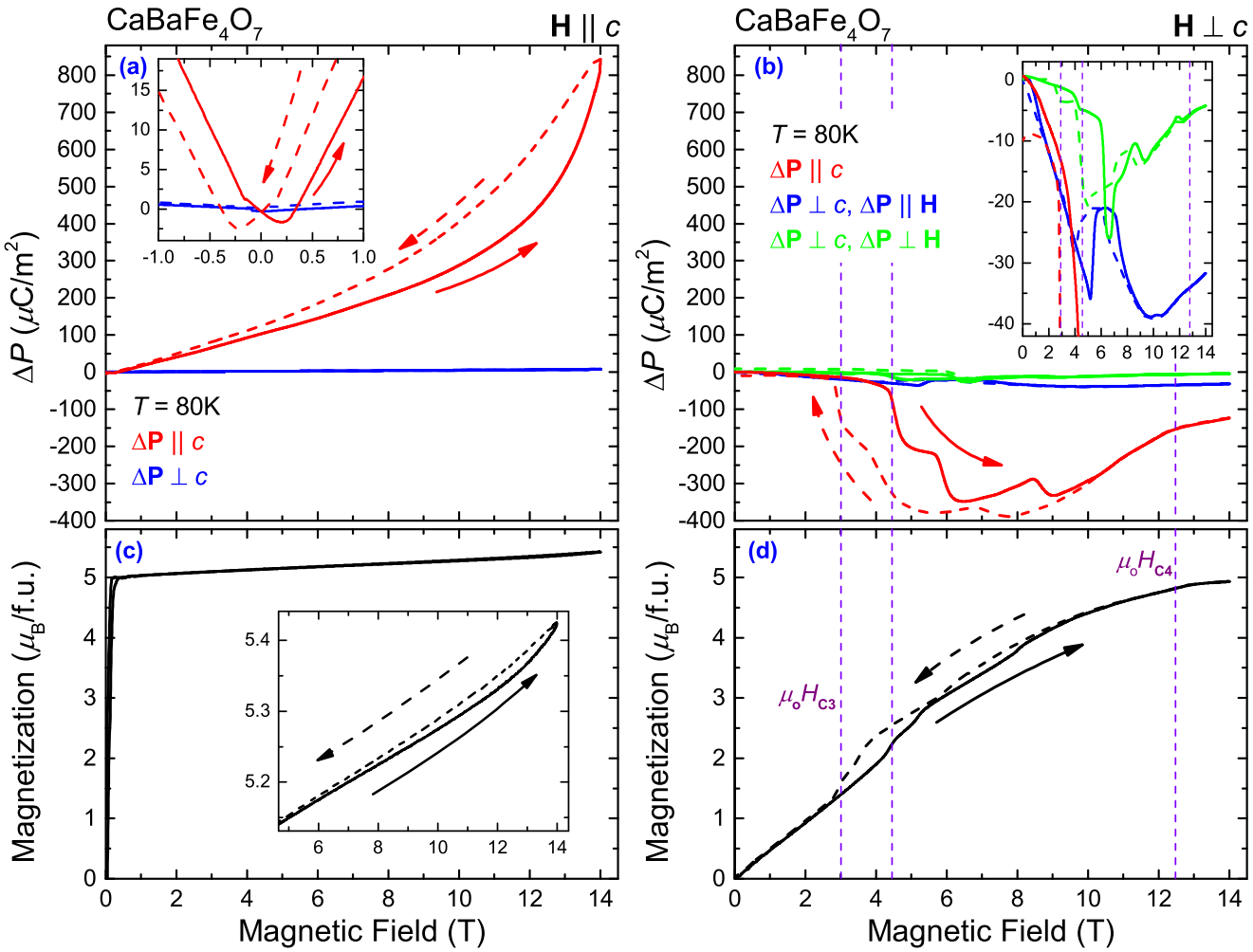

FIG. 5: (Color online) Magnetic-field dependence of the polarization change and corresponding magnetizations curves for magnetic fields applied along the c axis (panels a and c) and within the ab plane (panels b and d) at T=80 K. The largest change was observed in the c component of the polarization irrespective of the orientation of the magnetic field. The inset to (a) shows the symmetric butterfly loop in $\mathbf{\Delta P} \parallel c$ in the -1 T $\leq \mu_o H \leq$1 T region. The inset to (b) shows the polarization changes perpendicular to the c axis plotted in an enlarged scale. In the inset of (c), c axis magnetization is magnified to show the hysteresis corresponding to that of the polarization change.

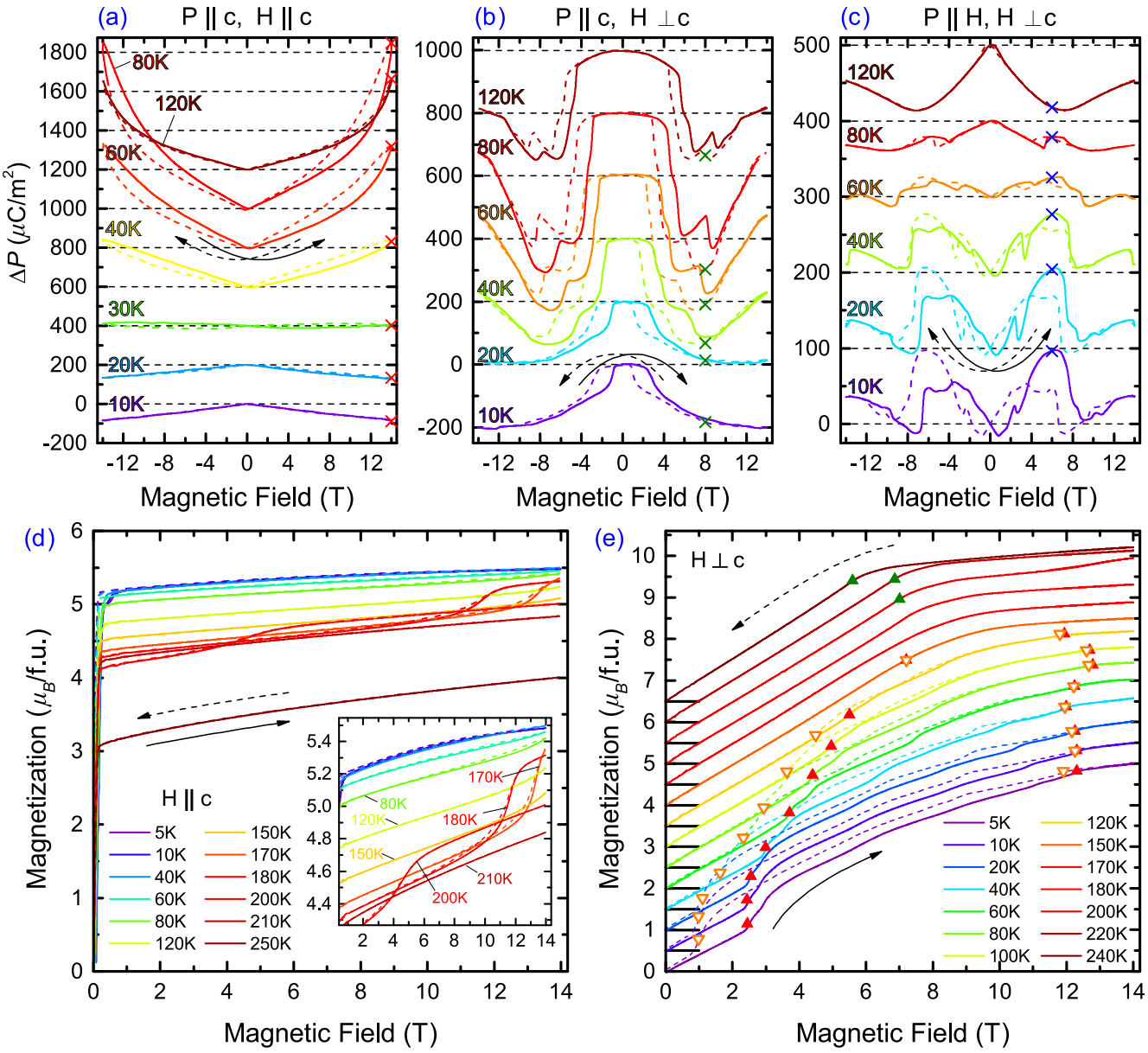

FIG. 6: (Color online) Magnetic-field dependence of polarization change ΔP at different temperatures, for (a) $\mathbf{\Delta P} \parallel c$ and $\mathbf{H} \parallel c$ axis, (b) $\mathbf{\Delta P} \parallel c$ and $\mathbf{H} \perp c$ axis, and (c) $\mathbf{\Delta P} \parallel \mathbf{H}$ and $\mathbf{H} \perp c$ axis. In panels (a), (b), and (c), each polarization curve is shifted vertically by 200 μC/m^2, 200 μC/m^2, and 100 μC/m^2, respectively, for the purpose of clarity. ΔP values marked by cross symbols are plotted in Fig. 7(b) against temperature. (d) Temperature dependence of the magnetization with the magnetic fields applied along the c axis. The inset shows a magnified view of the hysteresis region. (e) Temperature dependence of magnetization curves when the field is applied perpendicular to c. Each curve is shifted vertically by 0.5μ_B/f.u. for better visibility. Data collected increasing and decreasing magnetic fields, are plotted with solid and dashed lines, respectively. The magnetic phase transitions $\mu_o H_{C1}$, $\mu_o H_{C3}$ and $\mu_o H_{C4}$ are indicated by solid up and empty down triangles for the field increasing and decreasing runs, respectively. These phase transitions are determined as the local maximum of the $\frac{dM}{dH}$ curves, and are plotted in the $\mu_o H - T$ phase diagram by accordingly colored symbols (Fig. 8). For more details about the determination of the phase boundaries see Ref. [supplement].

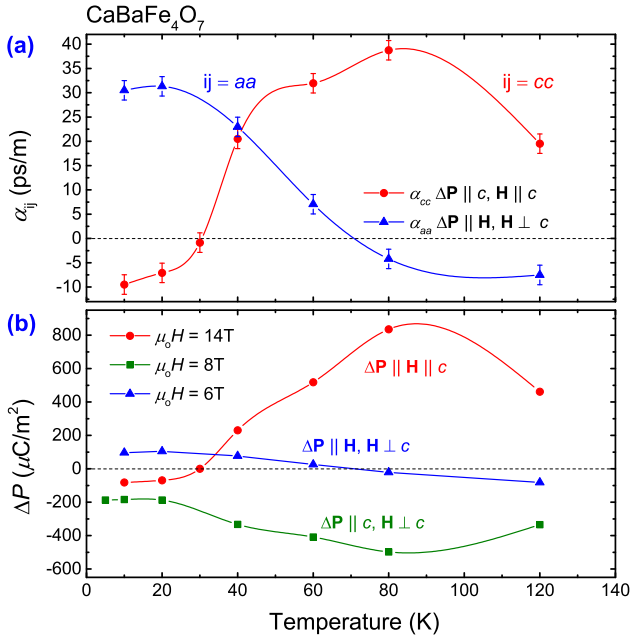

FIG. 7: (Color online) (a) Temperature dependence of the linear magnetoelectric susceptibilities $\alpha_{cc} = \frac{dP_c}{dH_c}$ and $\alpha_{aa} = \frac{dP_a}{dH_a}$ measured in the $\mathbf{\Delta P} \parallel \mathbf{H}$ configurations. (b) Temperature evolution of the maximums of the ΔP for the three configurations. The corresponding values are indicated by crosses in Figs. 6(a-c)).

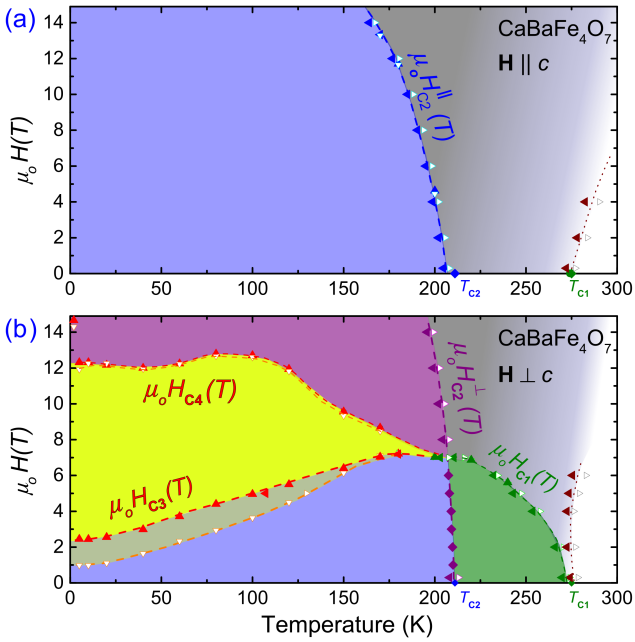

FIG. 8: (Color online) Temperature versus magnetic field phase diagram for fields applied (a) parallel and (b) perpendicular to the c axis. Phase boundaries based on magnetization measurements are represented by full or empty triangles, while those obtained from specific heat measurements are denoted by diamonds. Direction of the triangles illustrates the following measurement conditions: triangles pointing up and down correspond to isothermal magnetization measurements with increasing and decreasing fields respectively, while triangles pointing left and right indicate magnetization measurements at fixed external fields measured with decreasing and increasing temperatures, respectively. The yellow region in panel (b) covers the cascade of metamagnetic transitions. The phase boundaries are represented by dashed lines as guide to the eye. The crossover line connected to zero-field phase transition at T_{C1} is labeled with brown triangles. For detailed discussion of the different phase boundaries and their determination see the main text and the Supplementary material.